Active Microcantilevers for High Material Contrast in Harmonic Atomic Force Microscopy

Andreas Schuh, *Student Member, IEEE*, Manuel Hofer, Tzvetan Ivanov, and Ivo W. Rangelow

***Abstract*— Atomic force microscope (AFM) probes are mechanical beams that can be used to simultaneously map topography and material properties. Upon contact of the tip with the sample surface at each cycle in the intermittent mode, higher harmonics are excited. The harmonics in the vicinity of higher eigenmodes are enhanced and present an amplified response, ultimately carrying information about the material properties. In this paper, active cantilevers with integrated actuation and sensing are used as a basis to create harmonic cantilevers for the signal-to-noise ratio improved measurement of time-varying forces. Focused ion beam milling is used to remove mass from specific areas in the cantilever such that the fundamental and higher eigenmodes are tuned toward each other. Two methods are tested, where the shape and location of mass removal is determined, first by simulation and second through an *in situ* approach. Higher harmonics of the harmonic cantilevers with piezoresistive deflection sensors indicate a significant response of up to 10% in respect to the first harmonic. The improved material contrast mapping abilities of the modified cantilevers are validated by characterization and AFM images. [2014-0260]**

***Index Terms*— Atomic force microscopy, enhanced material contrast, cantilever harmonics, active cantilever probes, cantilever topology optimization.**

I. Introduction

ATOMIC Force Microscopes (AFMs) have unique abilities to simultaneously map topography and material properties of a sample. High imaging resolution is achieved by a sharp tip attached to the free end of a mechanical cantilever. Since its invention in 1985 [1] the AFM has evolved into a versatile tool with various operational modes. Dynamic modes help to reduce the contact mode's damaging forces exerted on the sample. Such modes are based on the influence of the tip-sample forces on the cantilever's dynamic behavior. Its detection is used to retrieve information about the sample surface and to create feedback loops.

In the past, material property mapping has focused on phase detection of the first transverse resonance. The phase sensitivity to compositional variations of the sample is generally accounted to non-conservative tip-sample interactions [2]–[4]. Monitoring the phase of higher cantilever eigenmodes has improved the cantilever's material sensitivity [5], [6].

Recent methods involve the first and excited higher harmonics to simultaneously map topography and material properties [7]–[10]. In the intermittent mode the periodic impact of the tip onto the sample results in a non-linear tip-sample force interaction. The contact time of tip and sample hereby depends on the Young's modulus E [11], [12]. Such contact time determines the magnitudes of the excited higher harmonics. The first harmonic represents the average tapping force and depends on the cantilever and its actuation/set-point. Hence, it has a constant magnitude across different materials [13].

The periodic tip-sample force F_{ts} can be expanded into a Fourier series $F_{ts}(t) = \sum_{n=0}^{\infty} \alpha_n cos(n\omega_1 t) + \beta_n sin(n\omega_1 t)$ [13], [14]. The nth harmonic force is determined by

$$F_{ts_n} cos(n\omega_1 t + \Theta_n) = \alpha_n cos(n\omega_1 t) + \beta_n sin(n\omega_1 t), \quad (1)$$

where α_n, β_n are the Fourier coefficients, ω_1 the driving frequency and Θ_n the harmonic phase. The magnitude of a specific harmonic force is

$$F_{ts_n} = \sqrt{\alpha_n^2 + \beta_n^2}. \quad (2)$$

The Total Harmonic Distortion (THD), a measurement of such coupling, is typically in the range of a few percent [10], [15]. Imaging in liquid rather than air indicates a higher harmonic response that can be useful for the investigation of biological samples [7], [16]. It is desirable to quantitatively retrieve a sample's material properties from the higher harmonics, such as its stiffness [11]. However, this requires detailed knowledge of the overall AFM system. Hence, the cantilever's response is generally compared to a reference sample obtained beforehand.

Higher cantilever eigenmodes directly influence the harmonic excitation process [14], [15], [17], [18]. The frequencies of the higher transverse eigenmodes follow specific ratios in respect to the first eigenmode. According to the Euler-Bernoulli beam theory, the ratios of homogeneous rectangular cantilevers are 6.28:1 and 17.86:1 of the second and third in respect to the first eigenmode, respectively. As a result, the magnitudes of the nearby excited 6th and 18th harmonics are amplified. Enhancement of harmonic responses

Manuscript received August 26, 2014; revised March 13, 2015; accepted April 7, 2015. Date of publication May 19, 2015; date of current version September 29, 2015. This work was supported in part by the European Union's Seventh Framework Programme FP7/2007-2013 under Grant 318804 (SNM) and in part by the Zentrales Innovationsprogramm Mittelstand-Project under Grant KF2114205NT2. Subject Editor R. R. A. Syms. *(Corresponding author: Andreas Schuh.)*

The authors are with the Department of Microelectronic and Nanoelectronic Systems, Faculty of Electrical Engineering and Information Technology, Ilmenau University of Technology, Ilmenau 98684, Germany (e-mail: aschuh@mit.edu; manuel.hofer@tu-ilmenau.de; tzvetan.ivanov@tu-ilmenau.de; ivo.rangelow@tu-ilmenau.de).

Color versions of one or more of the figures in this paper are available online at http://ieeexplore.ieee.org.

Digital Object Identifier 10.1109/JMEMS.2015.2428677

1057-7157 © 2015 IEEE. Personal use is permitted, but republication/redistribution requires IEEE permission.
See http://www.ieee.org/publications_standards/publications/rights/index.html for more information.

and improvement of Signal-to-Noise Ratios (SNRs) during imaging can thus be achieved by matching higher eigenmodes with integer multiples of the imaging resonance.

Specifically matched harmonic cantilevers have been partially explored in the past. Sahin *et al.* have demonstrated matching the third eigenmode by creating holes in the cantilever during its fabrication. The matched higher harmonic is amplified, as tested on optically sensed cantilevers [19], [20]. AFM images indicate surface properties that are invisible otherwise. However, this fabrication method is plagued by a low reproducibility and yield, based on uncertainties in the fabrication process itself. A different approach by Sahin *et al.* is the fabrication of torsional harmonic cantilevers [21]. Excited torsional harmonics during imaging indicate higher SNRs as compared to transverse harmonics. Rinaldi *et al.* have included holes of different sizes and shapes for a general purpose demonstration of its capabilities, for example to minimize the squeeze film effect [22], [23]. The holes are calculated by the Rayleigh-Ritz energy method. Cantilevers used are piezo-electric actuated and optically sensed. In contrast, Li *et al.* have attached a concentrated mass at specific locations on the cantilever's surface [24]. The modification results in a match of the second and third transverse eigenmodes with the 5th and 15th harmonic of the first resonance, respectively. A proposed approach by Balantekin *et al.* uses an imaging frequency that is the first transverse eigenmode divided by an integer value. The first eigenmode is then used to capture and amplify the harmonic response [25]. Sadewasser *et al.* have fabricated cantilevers with a wider anchored part and a narrower free end, moving the higher resonances as close as possible to the first resonance [26]. As such, the higher resonances are better accessible for the bandwidth limited vibration sensing. The unnecessity of harmonic cantilevers for high sensitive imaging of soft materials in liquid has been reported by Xu *et al.* [27].

In this work, both second and third eigenmodes are simultaneously matched with nearby harmonics by an enhanced approach. The modifications are carried out in a Focused Ion Beam (FIB) as a post cantilever fabrication step. Two different methods are employed. The first one is based on the cantilever's known characteristics to obtain proper sizes and locations of holes beforehand through Finite Element Method (FEM) simulations. This method leads to a higher reproducibility, ultimately to a success with every processed cantilever. The second method is based on an in-situ modification, where the cantilever is actuated and sensed inside the FIB chamber. The milling process is carried out for short periods of time with consequent frequency sweeps, until the eigenmodes match desired frequencies. With both methods the hole locations are decided beforehand. Holes can either be placed in the vibrational mass or stiffness domain of the cantilever effecting each eigenmode's local kinetic or potential energy, respectively. This either increases or decreases each eigenmode's frequency, as further investigated in [15] and [23]. The numerical FEM is chosen based on the utilized cantilevers' non-homogeneity in both material and shape.

An alternative approach would be adding mass in specific shapes and locations along the beam. This introduces a frequency shift of the individual eigenmodes due to increased stiffness or mass, as thoroughly discussed in the area of cantilever based mass detection [28], [29]. However, this approach is not feasible since a considerable amount of deposited material would be necessary for a meaningful impact. This leads to long FIB processing times with large amounts of expensive source materials. Such depositions also incorporate other undesired materials present in the vacuum chamber. The resulting amorphous structure is of low and unpredictable stiffness.

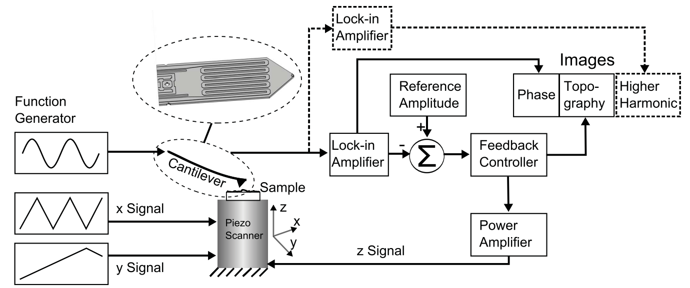

Fig. 1. Customized AFM setup including self-fabricated components. Dashed gray paths and boxes indicate the extension of the standard setup.

In the following, Section II describes the modified standard AFM setup used in this work. Section III outlines the cantilever FEM modeling process including the simulation of topological modifications. The consecutive FIB based fabrication including both digital mask and in-situ methods is described in Section IV. In Section V the harmonic cantilevers are characterized, evaluated towards their imaging performance and the results discussed. Conclusions are given in Section VI.

II. Specific Characterization and Imaging Setup

A customized commercial AFM setup is used for imaging and characterization of the fabricated harmonic cantilevers (Figure 1). An additional external Lock-in amplifier (Zürich Instruments HF2LI) is connected to demodulate the higher harmonics. The resulting signals and topography are simultaneously plotted within the AFM software to keep the dependencies on the lateral scan directions.

The active thermal bimorph actuated and piezo-resistive sensed cantilevers are developed by our group [30]–[32]. The bimorph effect based actuation is achieved by a combination of materials with different heat expansion coefficients. A meander shaped layer effectively dissipates an applied current into heat. This forces the cantilever layers to expand and then bend towards the material with the lower coefficient. The piezo-resistive stress sensors are located near the cantilever base and sense a tip displacement proportional signal. Four sensors forming a Wheatstone bridge are incorporated to increase the sensitivity. The cantilevers are fabricated through a series of micromachining processes involving consecutive steps of deposition, lithography, ion implantation and etching. The fabricated cantilever's layers consist of single-crystalline silicon with a thickness of about 5 μm, 700 nm thick SiO_2, a 500 nm thick Al meander and a final 200 nm Si_3N_4

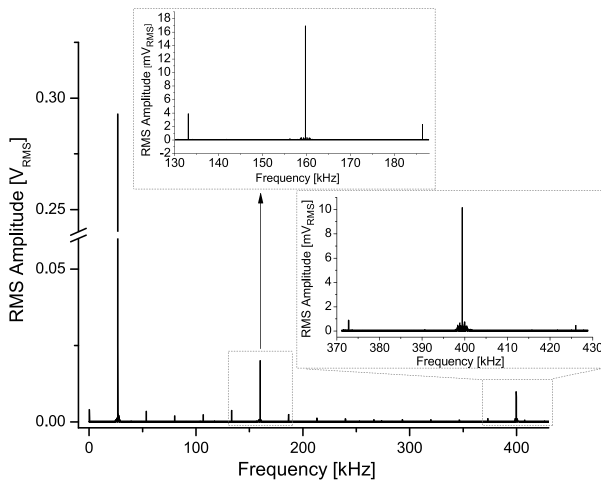

a)

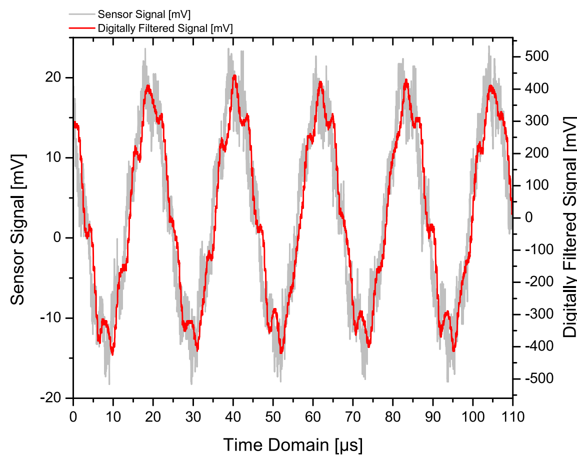

b)

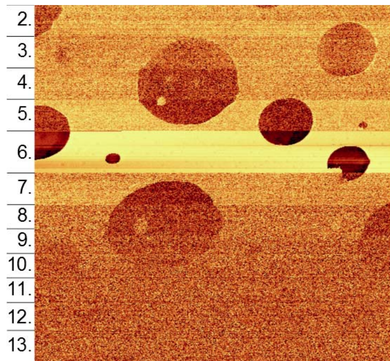

c)

Fig. 2. Different images show FFTs of harmonics, corresponding time domain signals and a harmonic sweep. a) FFT of the sensor signal indicating harmonics created in a cantilever in the intermittent mode and in the vicinity of a sample surface. b) Both raw and filtered cantilever time domain sensor signals show the first resonance and 6th harmonic superposed. c) Harmonic sweep of different frequencies created with approx. 40 lines each. The sections of the corresponding harmonics are indicated to the left of the image.

passivation on top. Nominal lateral dimensions are 360 μm in length and 140 μm in width with a sharp tip of 8 μm high.

Figure 2(a) indicates the excited harmonics of an active cantilever in the intermittent mode close to a sample surface and maintaining a specific set-point. Note that the ordinate

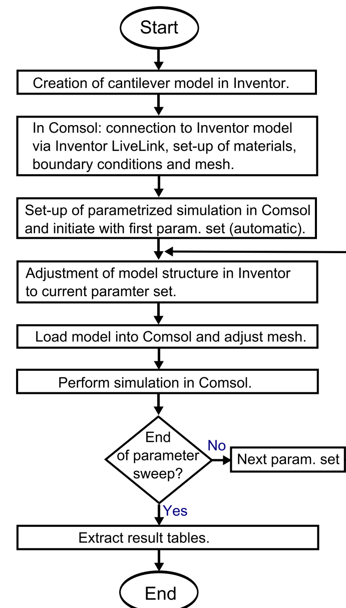

Fig. 3. Parameterized simulation cycle.

has a break as the first resonance's magnitude is larger than the introduced harmonics. However, the piezo-resistive sensor efficiently detects the harmonics with magnitudes of up to 10% of the first resonance. The enhanced harmonics close to cantilever eigenmodes are clearly visible. The fabricated active cantilevers may not follow the theoretical ratios of analytical models (Enhanced 15th instead of 18th harmonic in Figure 2(a)). Figure 2(b) presents raw and digitally filtered piezo-resistive sensor signals in time domain after its pre-amplification. The filtered signal is additionally amplified in respect to the raw signal to fit the analog-digital converters' ranges for an optimal resolution. In both cases, the excitation of the superimposed 6th harmonic is highly pronounced. The high Q factors of each eigenmode cause low damping of the higher harmonics' periodic excitation, as indicated in [15], [18], and [19]. Figure 2(c) is an image of various different harmonics. The sample is a Bruker PS-LDPE-12M, a two component polymer blend with different elastic moduli. It is used to indicate the harmonics' dependency on the sample stiffness. The Polystyrene (PS) appears as a film on the surface, whereas the Polyolefin Elastomer (LDPE) forms half-spheres. The PS and LDPE regions have Young's moduli of around 2 GPa and 0.1 GPa, respectively. For approx. 40 lines each, the 512 lines of the image represent the harmonics starting at the 2nd to the 13th one. As expected, the 6th harmonic is best pronounced.

III. Cantilever Modeling and Simulation

In this section, a three-dimensional model of the active cantilever is created and an eigenmode analysis performed by FEM simulations. The topological modifications are included in the simulation in a parameterized fashion. The prospective hole dimensions are swept according to a predefined range and step size. A milling structure is then chosen to introduce the proper modal shifts.

Figure 3 indicates the parametrized simulation cycle. In a first step, a model of the described cantilever is created in the CAD software Autodesk Inventor Professional. The 200 nm Si_3N_4X passivation layer is omitted as the dynamic behavior is dominated by the other layers. According to the simulation, the frequency ratios of the unmodified beam are 6.39:1 for the second to the first and 17.46:1 for the third to the first transverse eigenmode. The rectangular holes are then placed into the model with one or two sides variable during the simulation. A potential location is near the free end of the cantilever, where the nodes and thus stiffness domains of both second and third eigenmode are close to each other. The heating meander restricts the surface for mass removal to about 50 % of the total width. In addition, the area between the cantilever edge and outer wires is not included to be less prone to twisting. Although the active cantilevers impose some constraints regarding the shapes of holes, the overall milling effect is equivalent to using regular cantilevers without this restriction.

In a second step, the model is connected to the FEM simulation software Comsol Multiphysics via the LiveLink interface. A following parameterized simulation solves for the cantilever's eigenfrequencies and corresponding mode shapes based on variable hole sizes.

First, Comsol takes the model with initialized hole dimensions from the concurrent Inventor session. The model is then assigned with material properties, boundary conditions and a mesh, followed by the first simulation. Afterwards, Comsol assigns new parameters based on a given range and step size. These are communicated to Inventor, which in turn modifies the model. The modified model is sent back to Comsol and the mesh is automatically fitted to the new structure. This is followed by the next simulation. A completed parametrized simulation cycle consists of a set of different hole dimensions with corresponding eigenfrequency information. The count of individual simulations increases exponentially by using two or more variable parameters. Hence, the simulation complexity imposes a time constraint. Typically, our cantilever mesh consists of approximately 500.000 elements. This results in about 3-5 minutes per simulation on a Xeon 12-core Workstation.

In this work, we have performed simulations with various hole configurations. The different configurations modify the ratios with dissimilar slopes when compared to each other. A specific configuration is then chosen based on a target cantilever such that the desired ratios are achieved at similar hole sizes. This approach is necessary as the fabricated cantilevers often do not follow the theoretical frequency ratios. The true ratio of the second to the first eigenmode is mostly observed between 6.1:1 and 6.4:1. Similarly, the true ratio of the third to the first eigenmode is often between 16.5:1 and 17.2:1. Hence, the ratio of third to second eigenmode also depends on the cantilever.

The black curves in Figure 4 are an example indicating the modified frequency ratios obtained by the parameterized simulation. The length of the specific hole shapes is swept simultaneously and the width kept constant. The ratios of second and third eigenmodes to the first eigenmode change

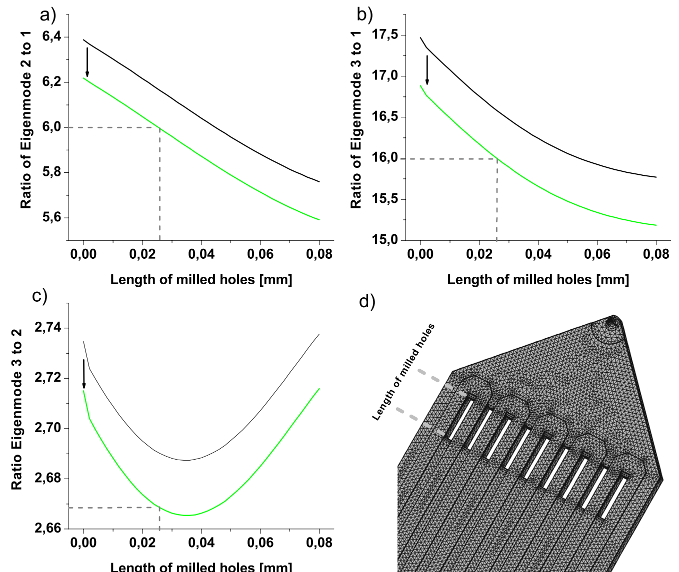

Fig. 4. Simulated ratios of the indicated transverse eigenmodes. The model in d) shows the hole configuration of the parameterized simulation to create a)-c). The black curve is the simulated frequency shift and the green curve its correction towards a specific real cantilever.

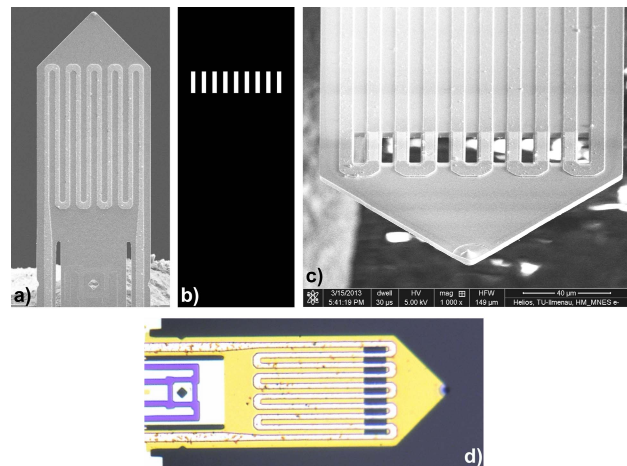

Fig. 5. a) SEM image of the cantilever before processing; b) Digital mask; c) SEM image of fabricated harmonic cantilever using cantilever of a) and mask of b); d) Cantilever of c) observed in an optical microscope.

linearly for a wide range of hole dimensions (black curves in Figure 4(a) and 4(b)). Note that in this case the required hole lengths are different in order to achieve the ratios of 6:1 and 16:1. However, as the truly required ratio shifts differ from the simulation this can be a potential fit with a real cantilever. A result is chosen that only removes as much material as needed to introduce the required ratio shifts in the real cantilever. Herby most cantilevers and their targeted modifications fall within the linear range.

The cantilever in Figure 5(a) has true ratios of 6.219:1 and 16.885:1. The simulated hole configuration of Figure 4 with a specific size is chosen to modify the ratios by 0.219 and 0.885 to receive ratios of 6:1 and 16:1, respectively. The green curves in Figure 4 are the adjusted frequency ratio shifts based on the true initial ratios of the real cantilever. Both desired frequency modifications are achieved by a

hole length of 26 μm (indicated by dashed lines). Hereby, the model's ratios are only lowered to 6.171 and 16.575, which is well within the linear domain of both ratios. The thereafter generated digital mask is shown in Figure 5(b). It is used in the following Section IV to modify the cantilever of Figure 5(a). The mask has a monochrome color coding, where black blocks and white requests a set FIB ion beam current.

IV. Fabrication of Harmonic Cantilevers

In the following, the two different fabrication strategies of modifying the cantilever dynamics are presented. In Method I the generated digital mask (bitmap) of Section III is used. Method II is carried out in-situ by performing repeated frequency sweeps and hereof based hole depth and area. In both cases, a Helios FEI 600i Dual Beam FIB is used. Alignment of its Ga^{+} ion beam to the electron beam allows alternating ion milling and non-invasive navigation/mask alignment.

Advantages of Method I are good repeatability and exactness of achieved ratios for every processed cantilever. Both factors depend on carefully measured cantilever characteristics and proper hole configurations. In contrast, Method II has a much lower repeatability and exactness. As the removal of mass influences each eigenmode differently it renders the result hard to predict on-the-go. A carefully chosen initial hole configuration and location is helpful. In addition, the frequency shifts are observed in vacuum with slightly different resonances than in air. Method I has a net process time of 1 - 5 min., whereas the manual procedure of Method II can take 30 minutes or more per cantilever. Method I requires preparation time for cantilever characterization and simulation. Although no such preparation needed with Method II it requires a suitable setup within the vacuum chamber. It includes electrical connections and a vacuum capable pre-amplifier.

A. Method I: Using a Digital Mask

The bitmap file is loaded into the FIB software and used as a milling mask by placing it on top of the cantilever. The milling time is a function of beam current (typically 10 nA), acceleration voltage (typically 10 kV), milling area and depth. Figure 5(c) shows the harmonic cantilever in the FIB chamber. Figure 5(d) is an optical image of the cantilever of Figure 5(c). Due to the cantilever fabrication process they can slightly vary in length, width and/or thickness. However, this can be corrected by properly aligning (stretching or quenching) the mask onto the cantilever, which adjusts for the shifted nodes.

Three additional milled cantilevers are shown in Figure 6(a)-(c). Figure 6(d) is a photo from inside the chamber with a mounted cantilever ready to be processed. In Figure 6(c), the milled holes are too wide, causing the undesired removal of the heating meander.

The milling process works well without using precursor gases. Those are often used to bind the sputtered material and avoid its deposition back to the sample. The SEM images of processed cantilevers indicate a contrast of the heating meander between milled holes. It is due to charges created and

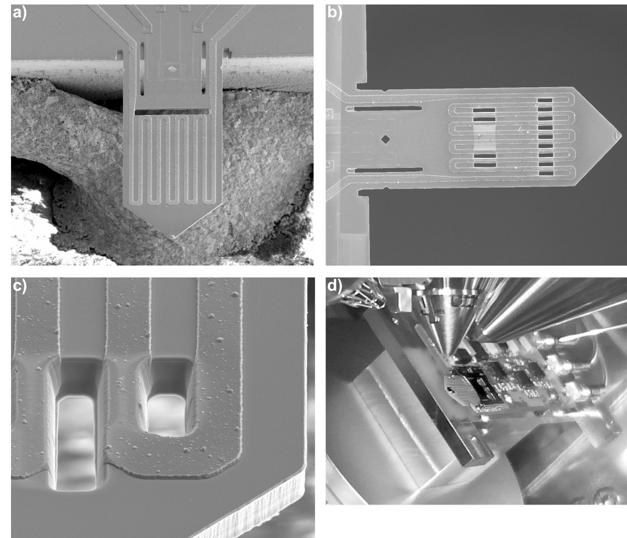

Fig. 6. a-c) Three additional milled cantilevers, d) photo from inside the chamber with a mounted cantilever. In c) the milling process caused the undesired removal of some of the aluminum meander layer.

trapped inside the top passivation layer. As will be confirmed in Section V this does not influence the resistance of the heating meander. This effect has been observed before as well as with a regular SEM. The FIB milling procedure is used as a parallel process, such that the heating meander is crossed over continuously. Setting the milling to a serial process might be able to prevent this effect.

B. Method II: In-Situ Approach by Observation

The cantilever can be modified by observing its frequency shifts in-situ. Here, the cantilever is mounted on a vacuum capable Printed Circuit Board (PCB) containing a pre-amplifier for the piezo-resistive sensor signal, as seen in Figure 6(d). All connections are routed to the ZI HF2LI outside the chamber that is used to obtain the frequency sweeps. Repeated sweeps are carried out to observe the shifts, while the ion beam is turned on for short times. Figure 7 shows frequency shifts at different milling stages for the first three resonances. In all subfigures, the first and second modification refers to the milled material between the heating meander and the large area towards the free end of the cantilever, respectively. Figure 7(c) shows cantilever images for corresponding frequency sweeps during milling near the free end (read from bottom to top). The difference between the first and second sweep is before and after milling between the meander.

Artifacts are caused by the configuration of piezo-sensor and vacuum pre-amplifier. The design of the pre-amplifier utilizes only one of the four resistors of the sensor bridge. This causes distortion of the shape of some resonances (for example top resonance in Figure 7(a)). It also causes the shape of some frequency sweeps to appear as dynamic zeros near the resonances (Figure 7). The artifacts disappear by using a pre-amplifier utilizing the full Wheatstone sensor bridge.

V. Cantilever Characterization, Imaging Results and Discussion

In this section, the resistances of the heating meander, frequency sweeps in air, mode shapes of the cantilever's

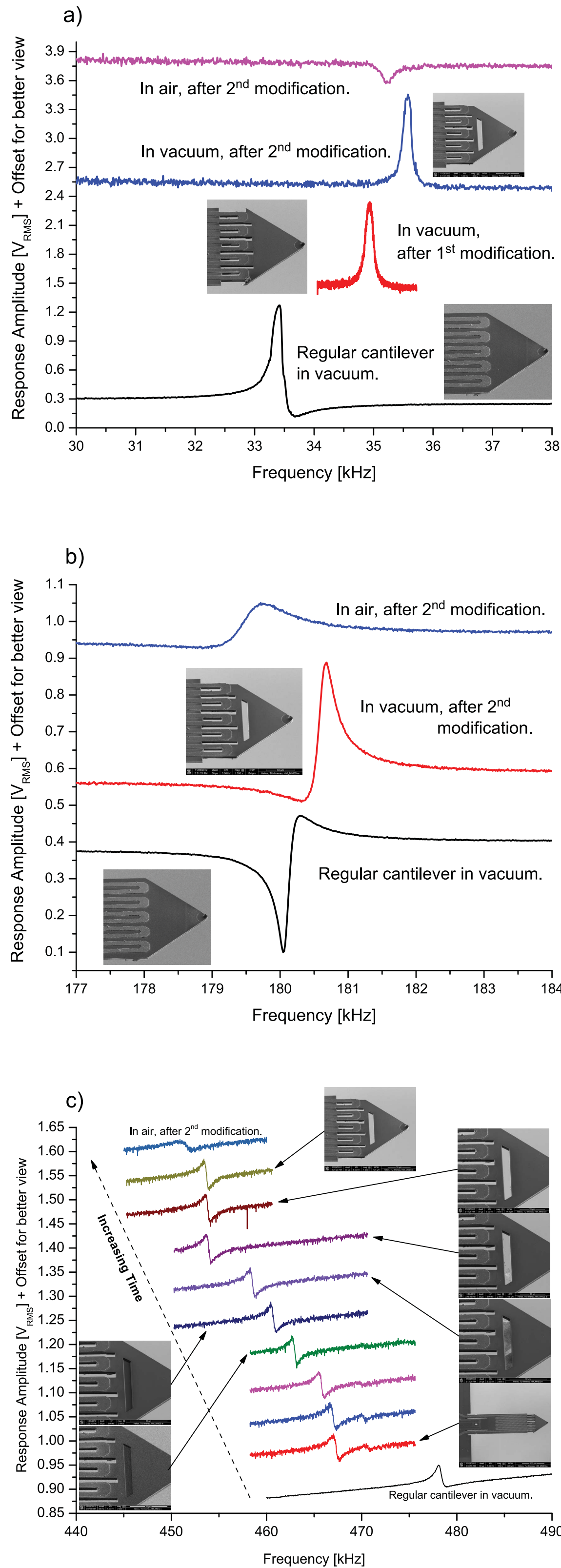

Fig. 7. Frequency shifts of the first three resonances during the modification in the FIB. All diagrams need to be read from the bottom to the top. a) 1th Eigenmode. b) 2nd Eigenmode. c) 3rd Eigenmode.

transverse resonances, enhancements in harmonic responses and imaging performances before and after the milling process are compared. The data presented in Subsections V-A and V-B are created with the same cantilever before and after the FIB process. In contrast, the data in Subsections V-C, V-D and V-E are obtained with the cantilever shown in Figure 5(c)/(d) and compared to an almost identical and unmodified cantilever. Initially, both of them were fabricated as direct neighbors on the wafer and are therefore very similar in their characteristics.

TABLE I
HEATING MEANDER RESISTOR VALUES BEFORE AND AFTER THE FIB MILLING

Cantilever in	Resistor value before milling	Resistor value after milling
Figure 5	25.8 Ω	25.8 Ω
Figure 6(a)	21.9 Ω	22.1 Ω
Figure 6(b)	25.9 Ω	26.2 Ω
Figure 7	25.8 Ω	25.8 Ω

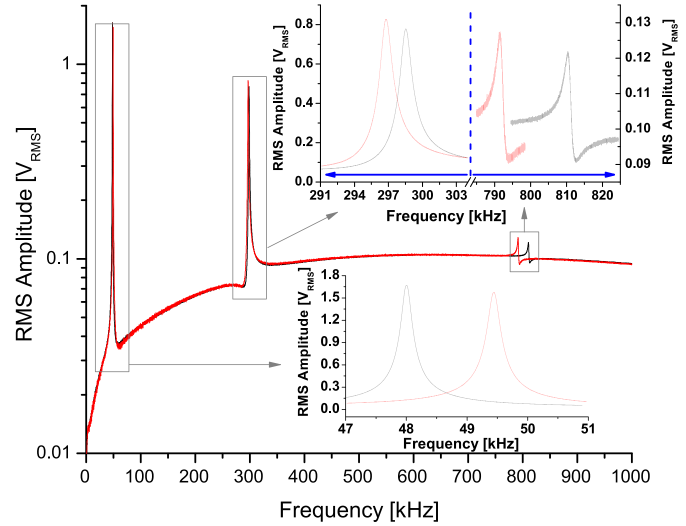

Fig. 8. Frequency sweeps of the active cantilever (Figure 5) before (black curve) and after (red curve) FIB milling. The inlets provide magnifications for a better view.

A. Resistances of the Heating Meander

It can be confirmed that resistances of the heating meander are not influenced by the milling process. The cantilever in Figure 5(c) indicates an altered contrast of the aluminum between the holes. Table I lists the resistances measured before and after the FIB modifications, referring to respective cantilevers shown in different figures. The values are matching, considering the measurement uncertainties, error of the measurement device, and slightly different contact resistances at the contact pads of each measurement.

B. Resonances

Frequency sweeps in air before and after the milling of the cantilever in Figure 5 are compared in Figure 8. The resonances before the modification are 48.004, 298.532 and 810.439 kHz. As discussed in Section III the original ratios are 6.219 and 16.883. After milling, the resonances have changed to 49.442, 296.781 and 791.488 kHz. The new

ratios of the second and third transverse eigenmode to the first eigenmode are 6.003 and 16.009 in air, respectively. Using similar actuation and sensing settings in the AFM, it can also be noted that the amplitude of the first resonance is slightly decreased after the FIB modification, as seen in Figure 8. Also, the two peak amplitudes of the higher resonances are slightly increased. A similar behavior has been observed on different FIB milled cantilevers.

The plot in Figure 8 indicates an amplitude roll-off towards lower frequencies. This is particularly pronounced in the presented logarithmic scale. It is caused by a High-Pass filter at the input of the AFM controller. This is to filter static cantilever sensor signals in dynamic AFM modes.

In the following, the frequency shifts of the cantilevers in Figure 6(a) and 6(b) are briefly indicated. All resonances of the cantilever in Figure 6(a) have decreased. Equivalently, the first, second and third resonance of the cantilever in Figure 6(b) are increased, decreased and decreased, respectively. Upon milling, one of the two eigenmode ratios changes more rapidly in respect to the other, as compared to the discussed cantilever of Figures 4 and 5. Such hole configurations can be necessary for different cantilevers depending on the initial ratios.

In ambient pressure the influence of the holes on the Q factors is evaluated. It is based on the shape of the resonance curves of a different cantilever. The center frequency of the resonance is divided by its bandwidth, evaluated at its half-power points (70.7% of peak amplitude) on both sides of the curve. The measurements are based on the same cantilever, obtained before and after the modification with the FIB. The Q factors for the first, second and third transverse resonances are reduced from 134 to 109, from 253 to 223 and from 286 to 278, respectively. As a comparison, the authors in [33] place holes in regular cantilevers to minimize the squeeze-film damping effect on the Q factor while being close to a sample surface.

C. *Modeshapes of the Cantilever Vibrations*

The shapes of the first three transverse cantilever eigenmodes without and with the modifications are compared with each other (Figure 9). The utilized harmonic cantilever is the one discussed in Section III and presented in Figure 5. In this case, the modification of the stiffness domain is dominant. It shifts the nodes of vibration and thus changes the mode shapes. This is most pronounced in the third eigenmode, where the nodes are considerably shifted towards the free end of the cantilever.

The curves are not always smooth as they carry uncertainties based on the measurement technique. A SIOS GmbH, Germany, interferometer (Nano Vibration Analyzer) with <0.1 nm resolution is mounted on an anti-vibration table. The laser is focused onto the cantilever, which in turn is mounted on a stage adjustable by three micrometer screws. During the experiment the cantilever is adjusted in steps of 10 μm along its length. This results in 36 to 38 measurements depending on the actual length of the cantilever. The major uncertainties in the measurement arise from the use of the micrometer screw, with a placement error estimated to be around ± 1 μm each interval. In addition, the start point at the free end of the cantilever can vary by a few micrometers. All diagrams in Figure 9 show an interruption with missing values close to the fixed end of the cantilever. It occurs when the interferometer laser hits the small stress concentration hole while it is moved along the centerline of the cantilever. For example, the hole can be seen in Figure 5(a). Figure 9(d) shows the 3-dimensional simulated transverse mode shapes of the active cantilever. They correspond to the measurements in Figure 9(a)-(c). Table II indicates the amplitude at the tip of each cantilever and transverse eigenmode that is used to normalize the mode shape. Hence, the values correspond to the value ‘1’ in the curves of Figure 9. The remaining amplitudes along the cantilever are hence proportionally scaled.

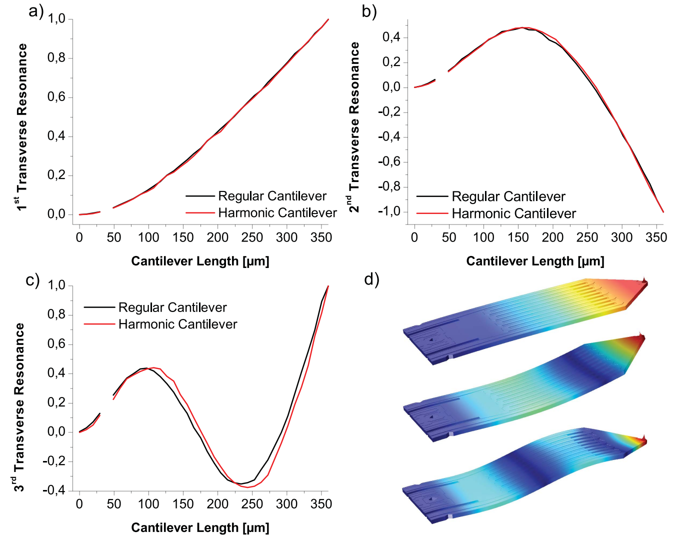

Fig. 9. Measured mode shapes of the first three transverse eigenmodes: a) First, b) second and c) third mode shape, respectively. 3-dimensional mode shape simulations of the harmonic cantilever are shown in d).

TABLE II
PEAK AMPLITUDES AT THE CANTILEVER TIPS USED FOR MODE SHAPE MEASUREMENTS AND NORMALIZATIONS

Regular cantilever	**Amplitude**
Eigenmode 1	211.3 nm
Eigenmode 2	71.1 nm
Eigenmode 3	10.5 nm
Harmonic cantilever	
Eigenmode 1	195.6 nm
Eigenmode 2	58.0 nm
Eigenmode 3	12.1 nm

D. *Amplification of Harmonics*

The amplification of the harmonics is demonstrated in the following. Each cantilever is actuated at its first resonance frequency. Here, the amplitudes in free air are 149 nm and 139 nm for the regular and harmonic cantilever, respectively. Both are then put into an intermittent contact with a sample surface. The distance is specified by a set-point of 35%. The sample is the Bruker PS-LDPE-12M as described in Section II.

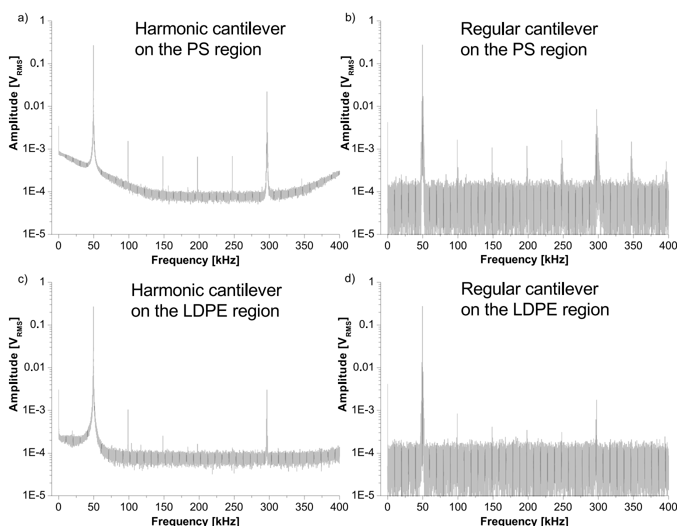

Fig. 10. Harmonic response of the harmonic and regular cantilevers tapping on the PS-LDPE-polymer sample at different locations that are indicated in the sub-diagrams. a) and b) are the harmonic and regular cantilever tapping on the harder PS region, respectively, c) and d) are the harmonic and regular cantilever tapping on the softer LDPE region, respectively.

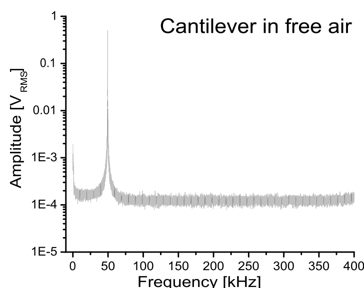

Fig. 11. FFT of the cantilever signals in free air.

A topographic image of the sample is taken to locate the different polymers. One at a time, the tip of each cantilever is placed on each polymer type. Here, the AFM is only used to control the distance of the tip to the sample without scanning the surface. The ZI HF2LI computes the 32768 points FFTs of each cantilever's sensor signals tapping the two different polymers. Note that the signals are measured right after their pre-amplification. Hence, the AFM controller's High-Pass filter with its roll-off present in Figure 8 does not influence the measurements.

Figure 10 shows the different FFTs. Figure 10(a) and 10(c) are obtained with the harmonic cantilever and Figure 10(b) and 10(d) with the regular cantilever. The sub-figures indicate the polymers measured with each FFT. In addition, the noise appears to be different for both cantilevers, visible due to the logarithmic scale. The regular cantilever's FFTs are obtained without averaging, whereas the harmonic cantilever's FFTs have an RMS averaging setting of 10 cycles. However, the FFTs are obtained after a steady state is reached during acquisition. The peaks around 50 kHz correspond to the first resonances and are constant in all cases, as it is used for distance feedback control.

For comparison, Figure 11 presents a typical FFT of the vibrating cantilevers in free air with the absence of excited harmonics.

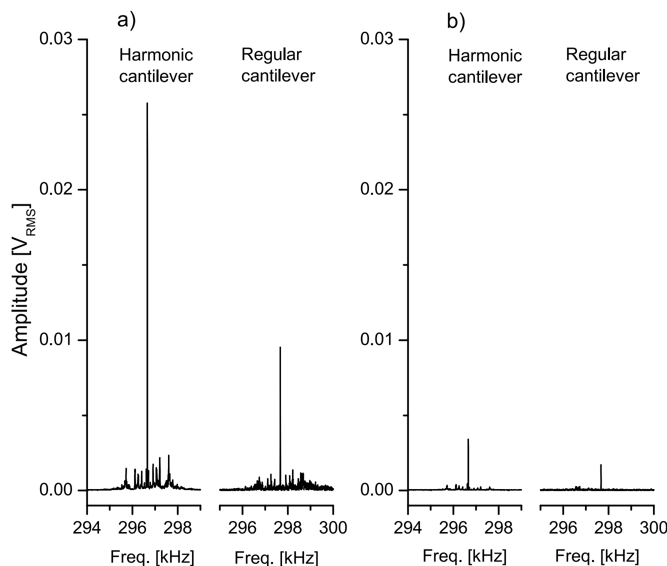

Fig. 12. Zoom into the 6th harmonics' responses of Figure 10 for better comparison and in a linear scale. The same two cantilevers are intermittently tapping on the a) PS and b) LDPE.

Figure 12 is a subset of Figure 10, where the 6th harmonics are shown on a linear scale for better comparison. Figure 12(a) and 12(b) compare the two cantilevers positioned on the PS and LDPE regions, respectively. On the PS region, the response of the harmonic cantilever has increased by 2.70 times compared to the regular cantilever; the response on the LDPE has increased by 1.99 times. As a note, the 6th harmonic of the harmonic cantilever reaches almost 10% of the first resonance's signal.

E. Imaging Results

The improvements in material contrast are shown in scanned AFM images. The sample under investigation consists of a silicon substrate with gold particles spun onto the surface. The cantilevers compared are the harmonic cantilever of Figure 5(c) and a regular cantilever similar in its characteristics, as discussed earlier in this section.

Two sets of images are taken with the setup of Figure 1, one with each cantilever. Each image set contains the topography and phase obtained with the first resonance as well as an image by monitoring the 6th harmonic (Figure 13). The latter is demodulated by the external ZI HF2LI Lock-in amplifier. It is locked onto the frequency that is 6 times higher than the first resonance frequency used for scanning. The magnitude of the 6th harmonic is plotted simultaneously with the other two images to keep the lateral dependencies.

In all cases the scan ranges are $(1.7\,\mu\mathrm{m})^2$ at a rate of 1 line/s and set-point of 35%. The free amplitudes of the first resonances are 88 nm and 95 nm for the harmonic and regular cantilever, respectively. The 6th harmonic of the regular cantilever (Figure 13(f)) does not indicate an increase in information compared to the topography or phase of the first eigenmode (Figure 13(d) and (e)). In contrast, the 6th harmonic of the harmonic cantilever (Figure 13(c)) shows various features between the gold particles that cannot be seen

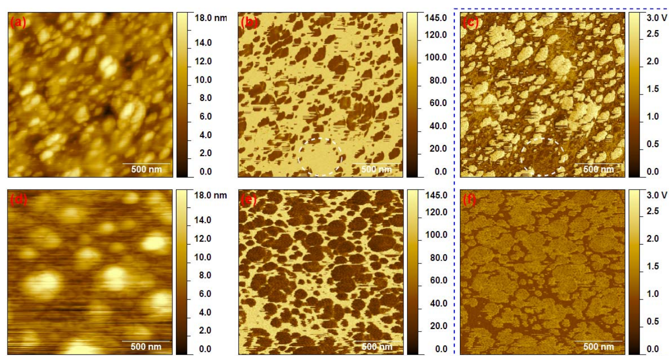

Fig. 13. (top row) are obtained with the harmonic cantilever, whereas (bottom row) are acquired with the regular cantilever. present the images of the topography obtained with the first resonances, their phases and the responses of the 6th harmonics, respectively.

in the topography or phase images (Figure 13(a) and (b)). An example area for comparison is indicated by dashed white circles. That contrast is assumed to originate from residuals of the fluid that contains and is used to spin the gold particles onto the silicon substrate. The harmonic cantilever is hence able to pick up these residues, whereas the regular cantilever is not.

On a last note, a small part of the contrast improvement achieved by extracting the higher harmonics can be attributed to the FIB modified cantilever parameters. As indicated in Section V-B the Q factors of all eigenmodes are lowered by 18% or less. This suggests increased tip-sample forces of the first transverse resonance tapping the surface and results in amplified higher harmonic signals. The lower Q factors in the higher eigenmodes lead to slightly increased harmonic excitations that damp out more quickly [18], [27]. Another factor is the modified dynamic stiffness of each eigenmode. However, in the first eigenmode the mass domain is mostly affected by the FIB modification.

VI. Conclusion

In this work, harmonic active cantilevers are created to enhance the material contrast of AFMs. It is based on the sample's excitation of higher harmonics dependent on the local material properties. Here, the SNR is improved by matching the cantilever's higher transverse eigenmodes with nearby harmonics. A FIB is used as a rapid prototyping tool to shift the eigenfrequencies of the cantilever. This is achieved by removing mass at locations specified by FEM simulations beforehand or in-situ during milling. The resulting cantilevers' harmonic responses are amplified and result in material contrast improvements during imaging. In addition, the higher harmonics of the piezo-resistive sensor based cantilevers show a significant response of up to 10 % of the first harmonic. This makes these cantilevers extremely suitable for the described method, as the response is much higher than of regular cantilevers reported in the literature. Our compact and fully integrated cantilevers can also be easily combined with fluid and vacuum environments. For example, this allows the observation of the dynamics of biological samples and their mechanical properties in fluid. As another example, the cross-linking effect of a microelectronic polymer resist upon lithography can be investigated in its locally modified stiffnesses.

A few future improvements of the presented work can be formulated. The parameterized simulation method utilized results in several simulation runs. This is required to obtain a set of masks to account for various different cantilevers. As a future step, we anticipate to introduce an automatic topology optimization. In that case, an objective function is minimized according to given criteria such that the targeted dynamic behavior and milling mask is found automatically for a given cantilever. In addition, the repetition of the frequency sweeps in Figure 7 can be replaced by a PLL based approach to track the resonance shifts in real-time.

Acknowledgment

The authors would like to thank the Department of Physical Chemistry and Microreaction Technology, Ilmenau University of Technology, for providing the gold particle sample and M. Kaestner for his help and discussion throughout the work.

References

[1] G. Binnig, C. F. Quate, and C. Gerber, "Atomic force microscope," *Phys. Rev. Lett.*, vol. 56, no. 9, pp. 930–933, 1986.

[2] J. P. Cleveland, B. Anczykowski, A. E. Schmid, and V. B. Elings, "Energy dissipation in tapping-mode atomic force microscopy," *Appl. Phys. Lett.*, vol. 72, no. 20, pp. 2613–2615, 1998.

[3] R. Garcia, C. J. Gomez, N. F. Martinez, S. Patil, C. Dietz, and R. Magerle, "Identification of nanoscale dissipation processes by dynamic atomic force microscopy," *Phys. Rev. Lett.*, vol. 97, no. 1, pp. 016103-1–016103-4, 2006.

[4] J. Melcher *et al.*, "Origins of phase contrast in the atomic force microscope in liquids," *Proc. Nat. Acad. Sci. USA*, vol. 106, no. 33, pp. 13655–13660, 2009.

[5] R. W. Stark, T. Drobek, and W. M. Heckl, "Tapping-mode atomic force microscopy and phase-imaging in higher eigenmodes," *Appl. Phys. Lett.*, vol. 74, no. 22, pp. 3296–3298, 1999.

[6] A. Ulcinas and V. Snitka, "Intermittent contact AFM using the higher modes of weak cantilever," *Ultramicroscopy*, vol. 86, nos. 1–2, pp. 217–222, 2001.

[7] A. Raman *et al.*, "Mapping nanomechanical properties of live cells using multi-harmonic atomic force microscopy," *Nature Nanotechnol.*, vol. 6, no. 12, pp. 809–814, 2011.

[8] M. Stark, R. W. Stark, W. M. Heckl, and R. Guckenberger, "Inverting dynamic force microscopy: From signals to time-resolved interaction forces," *Proc. Nat. Acad. Sci. USA*, vol. 99, no. 13, pp. 8473–8478, 2002.

[9] J. A. Turner and J. S. Wiehn, "Sensitivity of flexural and torsional vibration modes of atomic force microscope cantilevers to surface stiffness variations," *Nanotechnology*, vol. 12, no. 3, pp. 322–330, 2001.

[10] M. Stark, R. W. Stark, W. M. Heckl, and R. Guckenberger, "Spectroscopy of the anharmonic cantilever oscillations in tapping-mode atomic-force microscopy," *Appl. Phys. Lett.*, vol. 77, no. 20, pp. 3293–3295, 2000.

[11] R. W. Stark and W. M. Heckl, "Higher harmonics imaging in tapping-mode atomic-force microscopy," *Rev. Sci. Instrum.*, vol. 74, no. 12, pp. 5111–5114, 2003.

[12] L. Yuan, Q. Jian-Qiang, and L. Ying-Zi, "Theory of higher harmonics imaging in tapping-mode atomic force microscopy," *Chin. Phys. B*, vol. 19, no. 5, p. 050701, 2010.

[13] O. Sahin, C. F. Quate, O. Solgaard, and F. J. Giessibl, "Higher harmonics and time-varying forces in dynamic force microscopy," in *Springer Handbook of Nanotechnology*, B. Bhushan, Ed. Berlin, Germany: Springer-Verlag, 2010, pp. 711–729.

[14] R. W. Stark, "Spectroscopy of higher harmonics in dynamic atomic force microscopy," *Nanotechnology*, vol. 15, no. 3, pp. 347–351, 2004.

[15] R. W. Stark and W. M. Heckl, "Fourier transformed atomic force microscopy: Tapping mode atomic force microscopy beyond the Hookian approximation," *Surf. Sci.*, vol. 457, no. 1–2, pp. 219–228, 2000.

[16] J. Preiner, J. Tang, V. Pastushenko, and P. Hinterdorfer, "Higher harmonic atomic force microscopy: Imaging of biological membranes in liquid," *Phys. Rev. Lett.*, vol. 99, no. 4, p. 046102, 2007.

[17] R. Hillenbrand, M. Stark, and R. Guckenberger, "Higher-harmonics generation in tapping-mode atomic-force microscopy: Insights into the tip–sample interaction," *Appl. Phys. Lett.*, vol. 76, no. 23, pp. 3478–3480, 2000.

[18] T. R. Rodriguez and R. Garcia, "Tip motion in amplitude modulation (tapping-mode) atomic-force microscopy: Comparison between continuous and point-mass models," *Appl. Phys. Lett.*, vol. 80, no. 9, pp. 1646–1648, 2002.

[19] O. Sahin *et al.*, "High-resolution imaging of elastic properties using harmonic cantilevers," *Sens. Actuators A, Phys.*, vol. 114, nos. 2–3, pp. 183–190, 2004.

[20] O. Sahin, C. F. Quate, O. Solgaard, and A. Atalar, "Resonant harmonic response in tapping-mode atomic force microscopy," *Phys. Rev. B*, vol. 69, no. 16, p. 165416, 2004.

[21] O. Sahin, S. Magonov, C. Su, C. F. Quate, and O. Solgaard, "An atomic force microscope tip designed to measure time-varying nanomechanical forces," *Nature Nanotechnol.*, vol. 2, no. 8, pp. 507–514, 2007.

[22] G. Rinaldi, M. Packirisamy, and I. Stiharu, "Frequency tuning AFM optical levers using a slot," *Microsyst. Technol.*, vol. 14, no. 3, pp. 361–369, 2008.

[23] G. Rinaldi, M. Packirisamy, and I. Stiharu, "Tuning the dynamic behaviour of cantilever MEMS based sensors and actuators," *Sensor Rev.*, vol. 27, no. 2, pp. 142–150, 2007.

[24] H. Li, Y. Chen, and L. Dai, "Concentrated-mass cantilever enhances multiple harmonics in tapping-mode atomic force microscopy," *Appl. Phys. Lett.*, vol. 92, no. 15, p. 151903, 2008.

[25] M. Balantekin and A. Atalar, "Enhancing higher harmonics of a tapping cantilever by excitation at a submultiple of its resonance frequency," *Phys. Rev. B*, vol. 71, no. 12, p. 125416, 2005.

[26] S. Sadewasser, G. Villanueva, and J. A. Plaza, "Special cantilever geometry for the access of higher oscillation modes in atomic force microscopy," *Appl. Phys. Lett.*, vol. 89, no. 3, p. 033106, 2006.

[27] X. Xu, J. Melcher, S. Basak, R. Reifenberger, and A. Raman, "Compositional contrast of biological materials in liquids using the momentary excitation of higher eigenmodes in dynamic atomic force microscopy," *Phys. Rev. Lett.*, vol. 102, no. 6, p. 060801, 2009.

[28] J. D. Parkin and G. Hähner, "Mass determination and sensitivity based on resonance frequency changes of the higher flexural modes of cantilever sensors," *Rev. Sci. Instrum.*, vol. 82, no. 3, p. 035108, 2011.

[29] S. Dohn, R. Sandberg, W. Svendsen, and A. Boisen, "Enhanced functionality of cantilever based mass sensors using higher modes," *Appl. Phys. Lett.*, vol. 86, no. 23, p. 233501, 2005.

[30] R. Pedrak *et al.*, "Micromachined atomic force microscopy sensor with integrated piezoresistive sensor and thermal bimorph actuator for high-speed tapping-mode atomic force microscopy phase-imaging in higher eigenmodes," *J. Vac. Sci. Technol. B, Microelectron. Nanometer Struct.*, vol. 21, no. 6, pp. 3102–3107, 2003.

[31] T. Ivanov, T. Gotszalk, T. Sulzbach, and I. W. Rangelow, "Quantum size aspects of the piezoresistive effect in ultra thin piezoresistors," *Ultramicroscopy*, vol. 97, nos. 1–4, pp. 377–384, 2003.

[32] M. Woszczyna *et al.*, "Micromachined scanning proximal probes with integrated piezoresistive readout and bimetal actuator for high eigenmode operation," *J. Vac. Sci. Technol. B, Microelectron. Nanometer Struct.*, vol. 28, no. 6, p. C6N12, 2010.

[33] A. Perez-Cruz, A. Dominguez-Gonzalez, I. Stiharu, and R. A. Osornio-Rios, "Optimization of Q-factor of AFM cantilevers using genetic algorithms," *Ultramicroscopy*, vol. 115, pp. 61–67, Apr. 2012.

Andreas Schuh received the B.Sc. degree in electrical engineering from the Trier University of Applied Sciences, Germany, in 2006; the M.Sc. degree in electrical engineering from the Ilmenau University of Technology, Germany, in 2009, in collaboration with the Lawrence Berkeley National Laboratory, Berkeley; and the Ph.D. degree in electrical engineering with the Ilmenau University of Technology, in 2015, in collaboration with the Massachusetts Institute of Technology, Cambridge, MA, USA. He is currently with the Palo Alto Research Center, Palo Alto, CA, USA, working on embedded fiber-optic sensing in battery packs. His research interests include multifrequency control techniques for cantilever dynamics, high-speed atomic force microscopy, cantilever topology optimization, alternative lithography methods, and battery state of charge/health sensing.

Manuel Hofer was born in Linz, Austria, in 1984. He received the Dipl.-Ing. (FH) degree in medical engineering from the Upper Austrian Research University of Linz, Linz, in 2008, and the Dr.Ing. degree in micro and nanoengineering from the Ilmenau University of Technology, Ilmenau, Germany, in 2014. The topic of his Ph.D. thesis was Atto to Zeptogram Sensors. In 2014, he joined nano analytik GmbH as a Staff Scientist, where he was responsible for the production of silicon-based nano and microsensors. In parallel, he is currently a Research Associate with the Department of Micro- and Nanoelectronic Systems, Faculty of Electrical Engineering and Information Technology, Ilmenau University of Technology. He is working for two European projects with a focus on the development, fabrication, and manipulation of novel sensors.

Tzvetan Ivanov, photograph and biography not available at the time of publication.

Ivo W. Rangelow received the M.S. and Ph.D. degrees in electronics from the University of Wroclaw, in 1979 and 1983, respectively. From 1983 to 1984, he was with the University of Muenster, where his research was focused on the development of ion and electron beam techniques. In 1985, he joined the Fraunhofer-Institute in Berlin, where he worked on X-ray lithography. In 1986, he joined the University of Kassel, where he was focused on the development of cantilever beam force sensors, microresonators, and novel fabrication techniques for microelectromechanical systems devices. In 2005, he joined the Ilmenau University of Technology. He was a Guest Professor with the University of Vienna, Wroclaw University, and the University of Berkeley. He has authored or co-authored over 300 scientific papers and holds 48 patents. He is currently the Director of the Institute of Micro- and Nanoelectronics with the Ilmenau University of Technology.